



This is a repository copy of *Mitochondria Targeting Non-isocyanate-based Polyurethane Nanocapsules for Enzyme-Triggered Drug Release*.

White Rose Research Online URL for this paper:  
<http://eprints.whiterose.ac.uk/134497/>

Version: Accepted Version

---

**Article:**

Pramanik, S.K., Sreedharan, S., Singh, H. et al. (6 more authors) (2018) Mitochondria Targeting Non-isocyanate-based Polyurethane Nanocapsules for Enzyme-Triggered Drug Release. *Bioconjugate Chemistry*, 29 (11). pp. 3532-3543. ISSN 1043-1802

<https://doi.org/10.1021/acs.bioconjchem.8b00460>

---

**Reuse**

Items deposited in White Rose Research Online are protected by copyright, with all rights reserved unless indicated otherwise. They may be downloaded and/or printed for private study, or other acts as permitted by national copyright laws. The publisher or other rights holders may allow further reproduction and re-use of the full text version. This is indicated by the licence information on the White Rose Research Online record for the item.

**Takedown**

If you consider content in White Rose Research Online to be in breach of UK law, please notify us by emailing [eprints@whiterose.ac.uk](mailto:eprints@whiterose.ac.uk) including the URL of the record and the reason for the withdrawal request.



[eprints@whiterose.ac.uk](mailto:eprints@whiterose.ac.uk)  
<https://eprints.whiterose.ac.uk/>

# Mitochondria Targeting Non-isocyanate-based Polyurethane Nanocapsules for Enzyme-Triggered Drug Release

Sumit Kumar Pramanik,<sup>\*a</sup> Sreejesh Sreedharan,<sup>b</sup> Harwinder Singh,<sup>a</sup> Mohsina Khan,<sup>c</sup>  
Karishma Tiwari,<sup>a</sup> Anjali Shiras<sup>c</sup>, Carl Smythe,<sup>d</sup> Jim. A. Thomas<sup>\*b</sup> and Amitava Das<sup>\*a</sup>

<sup>a</sup>*CSIR-Central Salt and Marine Chemicals Research Institute, Bhavnagar, Gujarat, India.*

*Email: [sumitpramanik@csmcri.res.in](mailto:sumitpramanik@csmcri.res.in); [a.das@csmcri.res.in](mailto:a.das@csmcri.res.in)*

<sup>b</sup>*Department of Chemistry, University of Sheffield, Western Bank, Sheffield, S3 7HF, UK.*

*Email: [James.thomas@sheffield.ac.uk](mailto:James.thomas@sheffield.ac.uk)*

<sup>c</sup>*National Centre for Cell Science, Pune University Campus, Ganeshkhind, Pune- 411 007,  
Maharashtra, India*

<sup>d</sup>*Department of Biomedical Science, University of Sheffield, Western Bank, Sheffield, S3  
7HF.*

Sumit Kumar Pramanik and Sreejesh Sreedharan has equal contribution.

## ABSTRACT

Surface engineering of nanocarriers allows fine tuning of their interactions with biological organisms, potentially forming the basis of devices for the monitoring of intracellular events or for intracellular drug delivery. In this context, biodegradable nanocarriers or nanocapsules capable of carrying bioactive molecules or drugs into the mitochondrial matrix could offer new capabilities in treating mitochondrial diseases. Nanocapsules with a polymeric backbone that undergoes programmed rupture in response to a specific chemical or enzymatic stimulus with subsequent release of the bioactive molecule or drug at mitochondria would be particularly attractive for this function. With this goal in mind, we have developed biologically benign nanocapsules using polyurethane-based, polymeric backbone that incorporate repetitive ester functionalities. The resulting nanocapsules are found to be highly stable and monodispersed in size. Importantly, a new non-isocyanate route is adapted for the synthesis of these non-isocyanate polyurethane nanocapsules (NIPU). The embedded ester linkages of these capsules' shells have facilitated complete degradation of the polymeric backbone in response to a stimulus provided by an esterase enzyme. Hydrophilic payloads like rhodamine or doxorubicin can be loaded inside these nanocarriers during their synthesis by a interfacial polymerization reaction. The post-grafting of the nanocapsules with phosphonium ion, a mitochondria-targeting receptor functionality, has helped us achieve site-specific release of the drug. Co-localization experiments with commercial mitotracker green as well as mitotracker deep red confirmed localization of the cargo in mitochondria. Our in-vitro studies confirm that specific release of doxorubicin within mitochondria causes higher cytotoxicity and cell death compared to free doxorubicin. Endogenous enzyme triggered nanocapsule rupture and release of the encapsulated dye is also demonstrated in a zebrafish model. The

results of this proof-of-concept study illustrates that NIPU nanocarriers can provide a site-specific delivery vehicle and improve the therapeutic efficacy of a drug or be used to produce organelle-specific imaging studies.

**Keywords: Nanocapsules, Non-isocyanate polyurethane, Mitochondria, Structured illumination microscopy, Enzyme-Triggered, Interfacial reaction, Cellular uptake, Doxorubicin, Zebrafish.**

## **INTRODUCTION**

Mitochondria are the powerhouse of cells that provide energy for the survival of all eukaryotic cells.<sup>1-2</sup> This vital intracellular organelle is involved in different biological processes, including cell growth, cell differentiation, triggering of cell apoptosis and cell signaling.<sup>3-6</sup> Mitochondria dysfunction is associated with various human diseases such as cancer,<sup>7-8</sup> obesity, cardiac problem,<sup>9-10</sup> and Alzheimer's diseases.<sup>11-12</sup> One of the most challenging problems in the development of a therapeutic strategy for treating mitochondrial dysfunction lies in specific localization or distribution of these drugs within the mitochondria of live cells.<sup>13-15</sup>

In recent years, different kinds of mitochondria-targeted nanosystems have been developed, including small molecules and peptides, polymeric nanoparticles, liposomes, dendrimers, and micelles.<sup>16-21</sup> Among these approaches, due to their relatively thick, robust, and low permeability membranes, polymeric nanocapsules often offer superior stability and controlled release profiles,<sup>22-27</sup> for these reason their use in therapeutics and clinical diagnostics is growing. Potentially, they offer unlimited opportunity for encapsulation of useful compounds ranging from hydrophobic to hydrophilic drugs, small RNAs, inorganic nanoparticles and imaging/contrast agents.<sup>22, 25, 28-29</sup> Additionally, nanocapsules protect their payload from the external environment or *in-vivo* degradation and can provide site specificity for the controlled release of encapsulated payload.<sup>30-34</sup>

Construction of nanocapsules that meet all these criteria would significantly improve the efficacy of drug delivery systems. Considering this, the synthesis of novel biocompatible polymers has become an area of intense research.<sup>24</sup> Synthetic biodegradable polymers such as saturated polyesters, poly(lactide), polyurethane, poly(lactide-co-glycolide), and poly( $\epsilon$ -caprolactone) are typically utilized as drug carriers due to their biocompatibility and low *in-vivo* toxicity.<sup>24, 35-36</sup> In this context,

polyurethane has attracted much attention in biomedical research, due to its high elasticity, biocompatibility, chemical resistance, sterilizability, excellent strength and high elastic memory for maintaining tension.<sup>37-39</sup> A range of biomedical devices such as vascular grafts, cardiac valves, catheters, mammary prostheses, stents, intravaginal rings, bacterial cell detector and ocular implants have been prepared from polyurethanes.<sup>40-42</sup>

Nevertheless, one of the disadvantages of conventional polyurethane is that it is synthesized through the nucleophilic addition of hydroxyl and isocyanate moieties to yield urethane (–NH–CO–O–) linkages, as isocyanates are potentially carcinogenic and also highly moisture sensitive in nature.<sup>43,44-45,46</sup> Furthermore, significant amounts of opaque polyurea, which is not conducive to imaging applications is produced as a side-product during this reaction. Therefore, the development of an environmentally benign synthetic strategy for polyurethanes, that avoids the use of isocyanate derivative, is of great interest. Literature reports suggest that non-isocyanate polyurethanes (NIPUs) can be obtained by the reaction of multifunctional cyclic carbonates with aliphatic polyamines;<sup>45, 47</sup> in NIPUs the polymerization proceeds through ring opening of five-membered cyclic carbonates by diamines, forming the poly hydroxy urethane polymer backbone.<sup>47</sup> The presence of the ester functionality in the backbone of the NIPUs provides a mechanism for the programmed rupture of the polymeric backbone and subsequent controlled release of drug molecules in mitochondria through a biochemical transformation induced by esterase enzymes. Literature reports suggest that these enzymes are known to be concentrated inside cellular cytoplasm and are explicitly chosen as the biochemical trigger for degrading the nanocapsules.

Another burgeoning area of biomedical research is the development of imaging technologies for living systems. Modalities such as ultrasound, magnetic resonance, nuclear imaging, and particularly real-time fluorescence microscopy are attractive in

such studies as they allow interactions to be monitored with minimal disturbance of the biological environment.<sup>29, 48-52,53</sup> However, the major limitation of conventional optical microscopy is its moderate spatial resolution. Thus, many features of subcellular organelles and nanomaterials are poorly rendered, meaning that it is often not possible to study interactions at the nanomaterial–biomolecular interface. Recently the use of super-resolution techniques such as structured illumination microscopy (SIM) has offered the opportunity to provide insights into these complex interactions.<sup>54-55</sup>

Polymeric nanocapsules can be prepared by using numerous methods such as spray drying, double emulsion, nanoprecipitation, coacervation, and (micro-, mini-) emulsion polymerization.<sup>56-59</sup> Among these methodologies, inverse miniemulsion has been most popular as it allows effective encapsulation of both hydrophobic and hydrophilic entities.<sup>58-59</sup> For example, it offers an excellent route for the encapsulation of hydrophilic payloads in an organic solvent. Nanocapsules with the desired payload can then be subsequently transferred to aqueous phase.<sup>59-60</sup> Because of the negative membrane potential of the mitochondrial inner membrane, positively charged compounds (surfactants or ionic liquids) can accumulate in the mitochondrial matrix against their concentration gradient.<sup>61</sup> Thus, various lipophilic cations, including alkyl triphenylphosphonium cations, cyanine cations, cationic peptides and cationic ionic liquids can be attached to nanocarriers to improve their mitochondrial uptake.<sup>62-63</sup> The benefits of alkyl triphenylphosphonium cation based mitochondrial targeting over other approaches include their stability in biological systems, a combination of lipophilic and hydrophilic property, the low chemical reactivity toward cellular components, lack of light absorption or fluorescence in the visible spectral region and the relatively synthesis and purification.<sup>62, 64</sup>

Herein we report a strategy for developing mitochondria targeting nanocarriers that is suitable for the encapsulation inside its hydrophobic core of small drug molecules like doxorubicin. We have adopted a new non-isocyanate-based polyurethane synthesis methodology for the generation of nanocapsules with a repetitive ester functionality in their polymeric backbone. After loading with doxorubicin, post-grafting with mitochondria targeting triphenylphosphonium derivative ensures the nanocarriers specifically localize in mitochondria. Rupture of the ester functionalities in the polymeric backbone is achieved through a biochemical transformation induced by an esterase enzyme which specifically releases the drug doxorubicin within mitochondria. The controlled release of encapsulated cargo is also demonstrated within live zebrafish model. These results illustrate that the nanocarrier released drug avoids nonspecific uptake into other organelles such as lysosome or endosomes and leads to increased potency compared to conventional treatment.

## **RESULTS AND DISCUSSION**

The inverse mini-emulsion technique was used to produce nanocapsules containing urethane linkages (Figure 1), following an interfacial poly-addition reaction between stoichiometric amounts of amine (1,8-diaminooctane) and carbonate (adipate bicarbonate or alkyl C10 diglycerol carbonate) as the respective bi-functional monomers. In this approach, a NaCl solution was used to build up the osmotic pressure of droplets in the continuous hydrophobic phase and rhodamine/doxorubicin was encapsulated in the hydrophilic core. To facilitate the permeation of the nanocapsules through the potential barrier of the mitochondrial membrane and to improve the mitochondrial targeting efficiency, nanocapsules were then grafted with alkylated triphenylphosphonium cation.

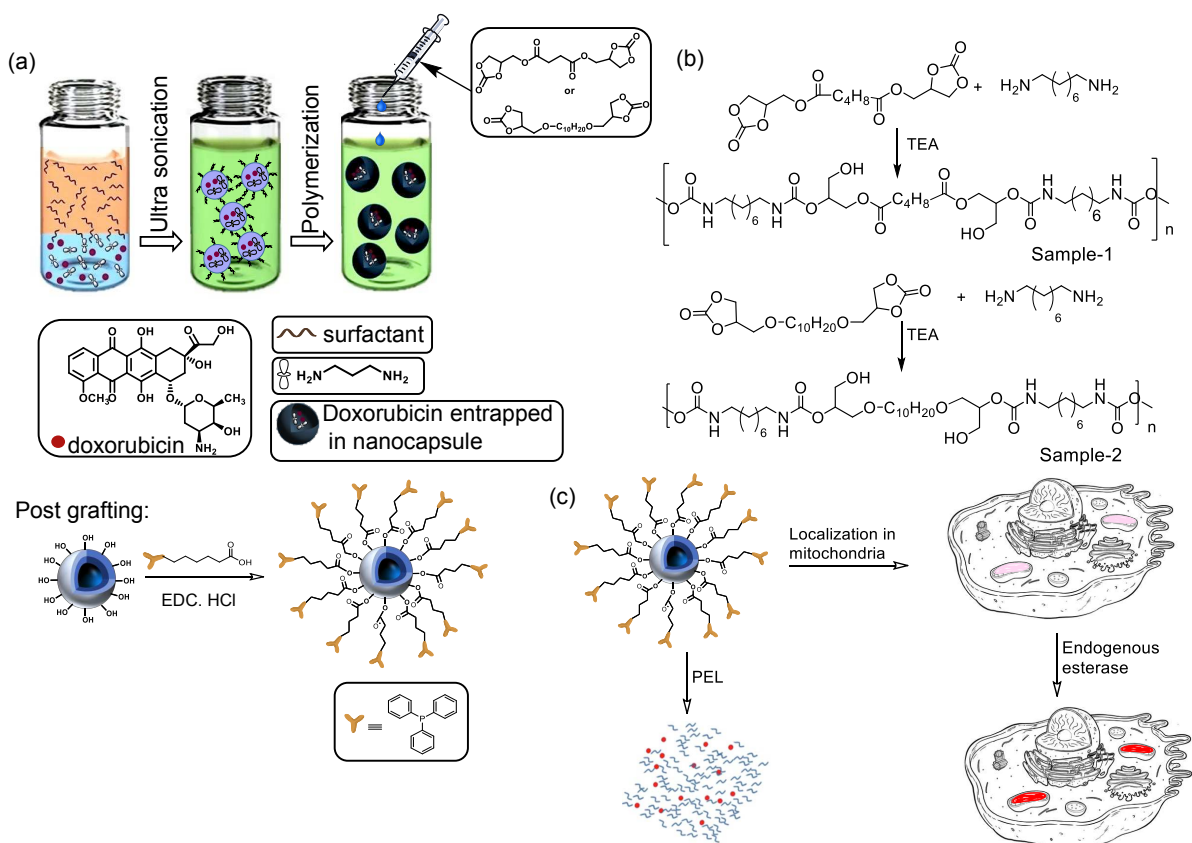


Figure 1. (a) The schematic representation of a base catalyzed interfacial polymerization reaction between amine and carbonate monomers in an inverse mini-emulsion. (b) Reaction scheme of polymer synthesis. (c) Schematic representation of enzymatic degradation and cellular uptake.

The stability of the resulting aqueous dispersion of nanocapsules was first checked optically for any visible phase separation. Colloidal stability, size, and polydispersity index (PDI) of these nanocapsules were also studied using dynamic light scattering (DLS), which revealed that the hydrodynamic diameter (intensity average) for both types of nanocapsule is around 250-260 nm with a polydispersity index  $\sim 0.25$ . The characteristics of the synthesized nanocapsules are summarized in Table 1. The low polydispersity indicates a narrow size distribution, and the sizes observed here are comparable to values reported for other polyurethane capsules.<sup>65</sup>

**Table 1.** Size, PDI, and chemical composition of the synthesized nanocapsules.

Capsule	Dispersed phase	Additive phase	Size / PDI (organic phase in DLS)	Size/ PDI (aqueous Phase in DLS)
Sample 1	0.57 mmol 1,8-diaminooctane, rhodamine / doxorubicin	0.57 mmol adipate bis carbonate, TEA	204nm / 0.06	248nm / 0.21
Sample 2	0.57 mmol 1,8-diaminooctane, rhodamine / doxorubicin	0.57 mmol alkyl C10 diglycerol carbonate, TEA	211nm / 0.07	261nm / 0.24

The overall success of the carbonate–amine reaction is confirmed by the presence of urethane groups detected in FT-IR spectra obtained from air-dried samples (Figure 2A). Typical bands at  $1535\text{ cm}^{-1}$  and  $1725\text{ cm}^{-1}$  are attributed to the N-H bending vibrations and the carbonyl group (C=O) stretching vibrations..<sup>66-67</sup>

The solid-state  $^{13}\text{C}$  NMR of the samples are presented in Figure 2B. Signals for aliphatic carbons appear within the range 21 - 46 ppm. While the peak at 70 ppm originated from the alcohol and the ether functionalities of the carbonate monomer, the small peak at 175 ppm was attributed to the carbonyl carbon of the ester functionality of the carbonate monomer.<sup>68</sup> However, a well-defined, intense peak at 157 ppm corresponds to the carbonyl carbon of urethane linkages.<sup>69</sup> The morphology of the nanocapsules was studied using both SEM and TEM microscopic techniques .

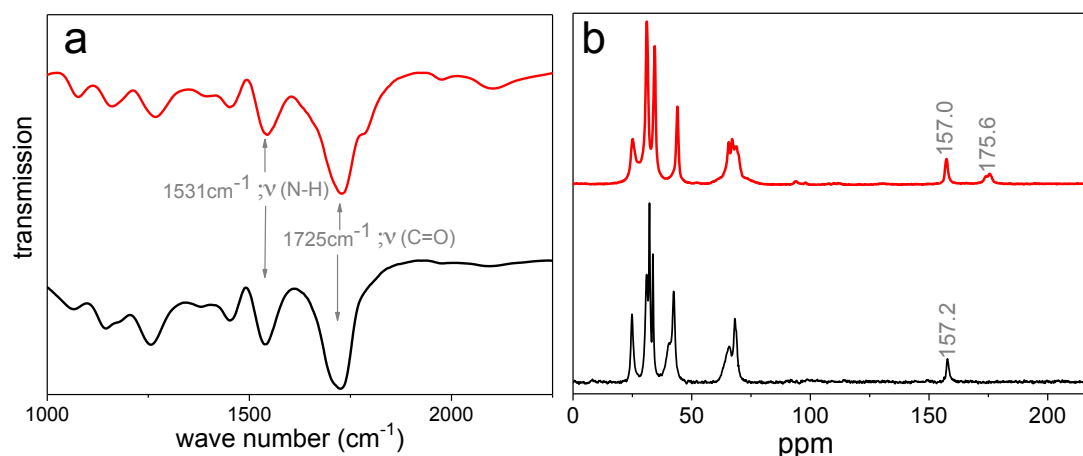


Figure 2. (a) Transmission FT-IR spectra and (b) NMR showing the presence of and urethane linkages for all the samples 1 (red) and sample 2 (black).

TEM micrographs and analyses (Figure 3) confirmed the size of the nanocapsules to be around 200 nm with shell thickness in the range 12 - 19 nm, which agreed well with the results of previous reports.<sup>59</sup> The nanocapsules were redispersed in HEPES buffer solution and the colloidal dispersion was found to be stable. DLS studies revealed an enhanced hydrodynamic diameter for nanocapsules. The average size of aqueous nanocapsules was 250 - 260 nm with a PDI value of 0.25, exhibiting an increase in the size of around 50 nm as compared to the value measured in the organic phase. This expected increase in size after redispersion is attributed to the hydration of the hydrophilic acid and hydroxyl functionalities of the surfactant in the aqueous phase. Overall, the results of DLS, SEM, and TEM studies clearly confirm the formation of a stable aqueous dispersion of intact nanocapsules.

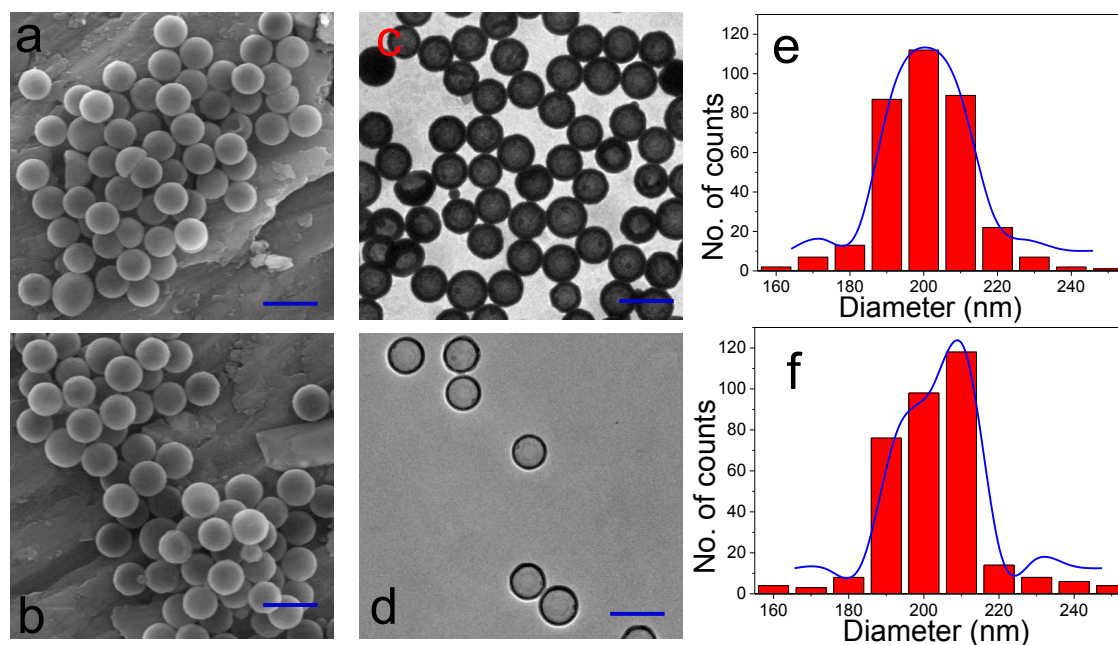


Figure 3. SEM and TEM (scale bar 300 nm) images: (a) and (b) are the SEM images for sample 1 and 2 respectively; similarly (c) and (d) are the TEM images for 1 and 2 respectively. Size distribution

of the nanocapsules obtained from TEM images for sample 1 (2) and sample 2 (f). Gatan Microscopy Suite Software was used for quantitative analysis and then the histogram was plotted in Ms excel. Data were obtained by measuring over 300 nanocapsules.

To develop insights into the organelle-specific localization of the surface modified nanocapsules, nanocapsules loaded with rhodamine as the cargo were used for optical microscopy. Interestingly, this rhodamine derivative was found to be highly compatible with the super-resolution (SR) technique, SIM. In SIM, a shifting grid pattern is generated through the interference of diffraction orders and superimposed on each collected frame, followed by processing of an image set to collect the final SR image. Whilst the practical limit of conventional optical microscopy is restricted to resolutions above  $\sim 250$  nm, SIM commonly provides resolution to around 100 nanometers. Relatively fast acquisition times and low light exposures compared to other stochastic SR techniques such as STORM, have made this technique most suited for 3-D sectioning.

Therefore, experiments on the uptake of the rhodamine loaded nanocapsules in LN229 cells after 2 hours incubation were carried out using SIM. The resulting images indicated that the nanocapsules largely localize in the cytosol of LN229 cells (Figure S1-S2, Supporting Information). While subsequent co-staining experiments with commercial probes revealed that the nanocapsules localize in a specific organelle.

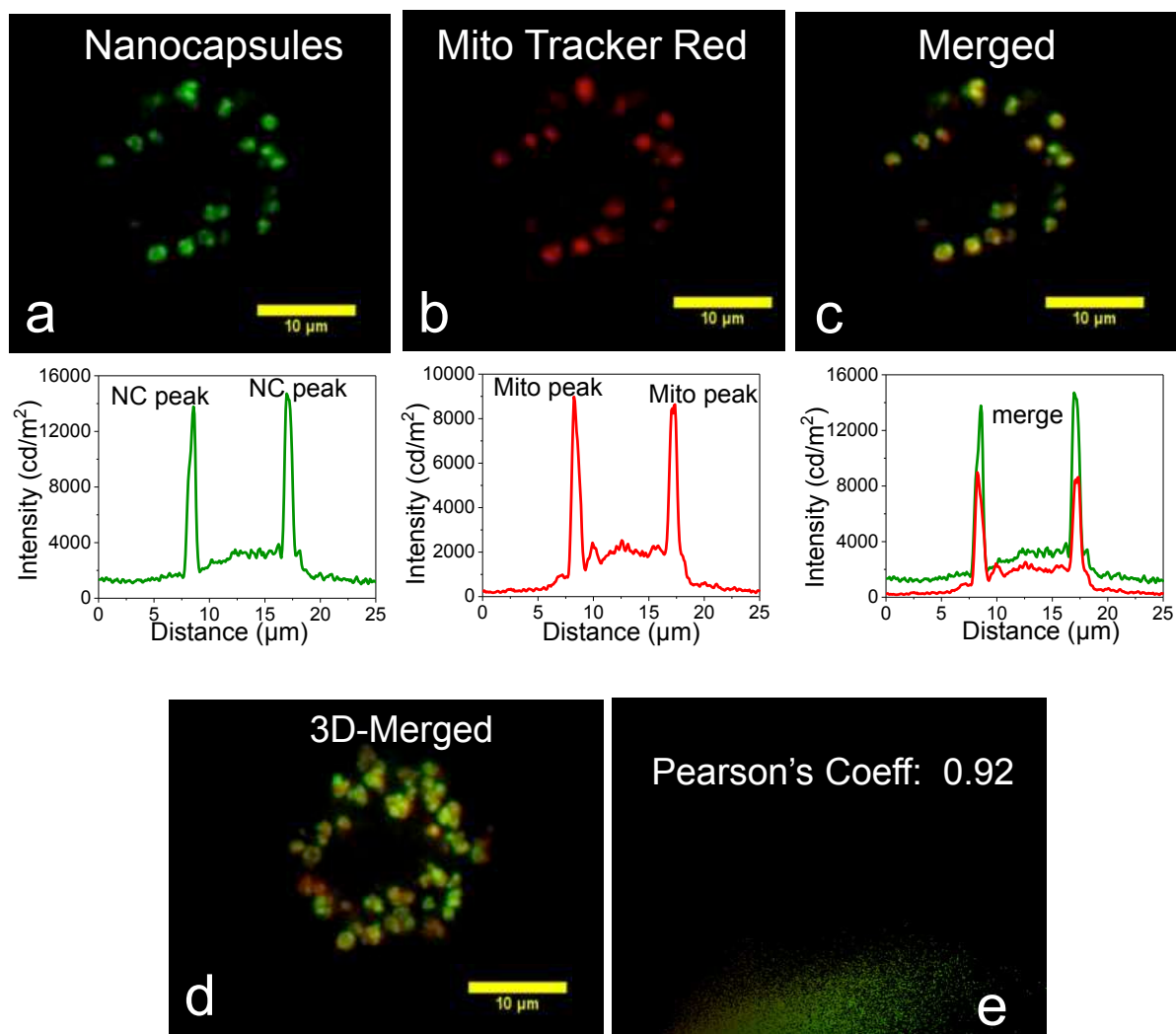


Figure 4. Colocalization experiments of intracellular localization of rhodamine green loaded nanocapsules using MitoTracker probes: Widefield microscopy images of in cellular emission of sample 2 (panel a) with intensity along the traced line shown underneath. Emission from Mito Tracker Deep Red (panel b) and intensity along the same line shown below. The overlap of the intensity is shown in panel c. panel c shows the overlap of the green and red fluorescence, indicating mitochondria localization of sample 2 nanocapsules. Panel d shows the Pearson co-efficient = 0.92. Scale bar 10 μm.

Unlike rhodamine, MTG and MTDR are not sufficiently photostable to be used used in SIM, as they undergo considerable photo bleaching in the required acquisition cycle. Therefore, co-localisation studies were carried out using deconvoluted widefield optical microscopy.

Co-treated cells show that the punctuated intracellular emission from the dye-loaded nanocapsules correlates strongly with the emission from MTDR (Figure 4b). The optical signals of MTDR and nanocapsule 2 were found to co-localize with a Pearson's Coefficient of 0.92 Figure 4e. Similar co-localization experiments with probes such as LysoTracker Deep Red (LTDR) and Hoechst 33258 confirmed specific mitochondrial localization (Figure 5 and S4 (supporting information)). For examples, studies with LTRD show very low Pearson's Coefficient of 0.0528.

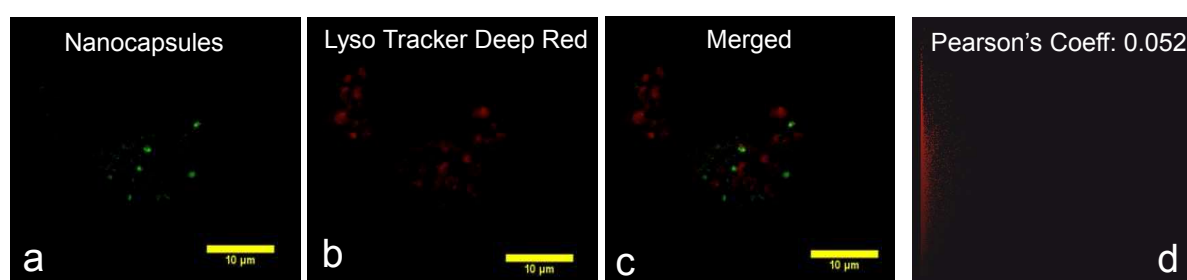


Figure 5. Colocalization experiments of Intracellular localization of sample 2 using Lyso Tracker probes: Widefield microscopy images of in cellular emission of nanocapsules (Panel a) and emission from Lyso Tracker Deep Red (Panel b). The overlap of the intensity is shown in Panel c. Panel c shows no overlap of the green and red fluorescence indicates that the nanocapsules are not localized over lysosomes. Panel d shows the Pearson coefficient = 0.052, also supports that. Scale bar 10  $\mu\text{m}$ .

After ascertaining cellular uptake, as well as subcellular localization of nanocapsules loaded with appropriate rhodamine-based dye or doxorubicin, we examined the stimuli-responsive rapture of the ester functionalities in the polymeric backbone with subsequent release of the cargo (dye or drug) release process induced by esterase from porcine liver (EPL). To determine this, both the nanocapsules were synthesized in the presence of a hydrophilic drug, doxorubicin. The effective encapsulation efficiency for these samples was calculated by a previously reported protocol and found to be in the range of 91-94 %.<sup>59</sup> The resulting nanocapsules were subjected to treatment with EPL [0.10 mL, 5 mg/mL solution in 4.0M

(NH<sub>4</sub>)<sub>2</sub>SO<sub>4</sub> at 37 °C] and time-dependent release of doxorubicin was monitored by probing the enhancement in fluorescence intensity (Figure 6). The nanocapsules (Sample -1) having ester linkages at the polymeric backbone were successfully cleaved and effected the release of the drug, doxorubicin in solution. This prevented the self-quenching phenomenon, which was otherwise operative when doxorubicin is encapsulated inside nanocapsules. *In-vitro* studies revealed an enhancement of 93 fold in emission intensity for the doxorubicin within 6 hours of incubation of the drug-loaded nanocapsules with EPL (Inset of Figure 6c). Control experiments using nanocapsule (Sample -2) without ester linkages in the polymeric backbone showed insignificant release of doxorubicin (Figure 6c). Thus, these results confirm that EPL can successfully cleave ester functionalities in the polymeric backbone with subsequent release of the drug.

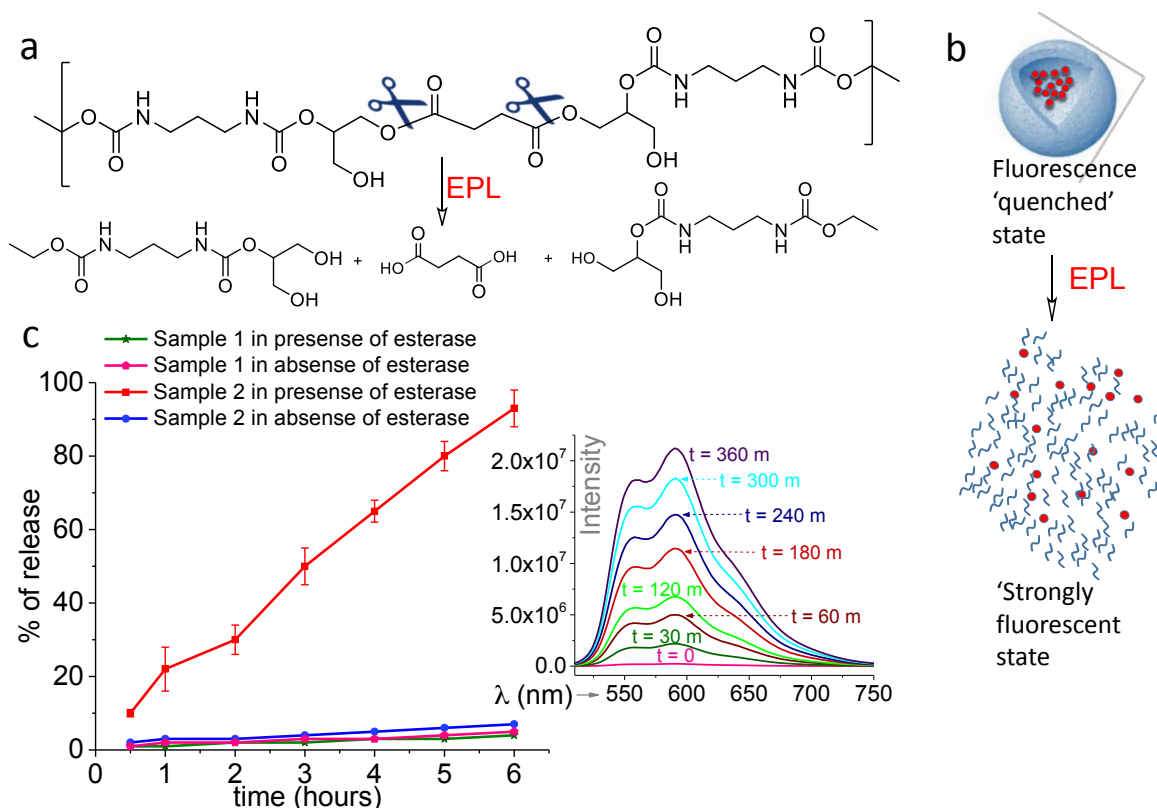


Figure 6. The enzyme-mediated release of nanocapsules internal cargo (doxorubicin). (a) and (b) Schematic representation for the degradation of capsule shell polymer by esterase enzyme. (c)

Representative plots of ester-linked nanocapsules (sample 1) versus nonester-linked nanocapsules (sample 2) versus time on esterase treatment, indicating that the esterase enzyme degrades the capsule shell for sample 1 (red color) and releases the doxorubicin, whereas - in absence of esterase enzyme - the release of doxorubicin is almost nil (blue color). The absence of ester linkages in the polymer shell of sample 2 means that it does not show any release of internal cargo (green color). The corresponding steady-state emission spectra are shown in inset.

After ensuring the efficiency of the esterase in fragmenting the biocompatible polymeric shell and achieving the subsequent release of doxorubicin, cellular studies with LN229 cells (glioblastoma, brain cancer) were initiated. Confocal studies showed that the nanocapsules were indeed readily taken up by cells.<sup>70</sup> The doxorubicin loaded nanocapsules (Figure 7a for sample 2 and Figure 7b for Sample 1) and pure doxorubicin (Figure 7c) were incubated with LN229 cells (glioblastoma, brain cancer) for 24 h at 37 °C. These microscopic images revealed that, after 24 hours incubation, the nanocapsules with no ester linkages (sample 2) cross the cell membrane and locate within mitochondria without degradation of the capsule shell (Figure 7a). Nanocapsules containing ester linkages (sample 1) degrade by endogenous esterase enzyme and release the encapsulated doxorubicin which gradually moves to the nucleus (Figure 7b). In a controlled experiment, with pure doxorubicin, after 4 hours incubation, all the doxorubicin crossed the cytosol and located to the nucleus.

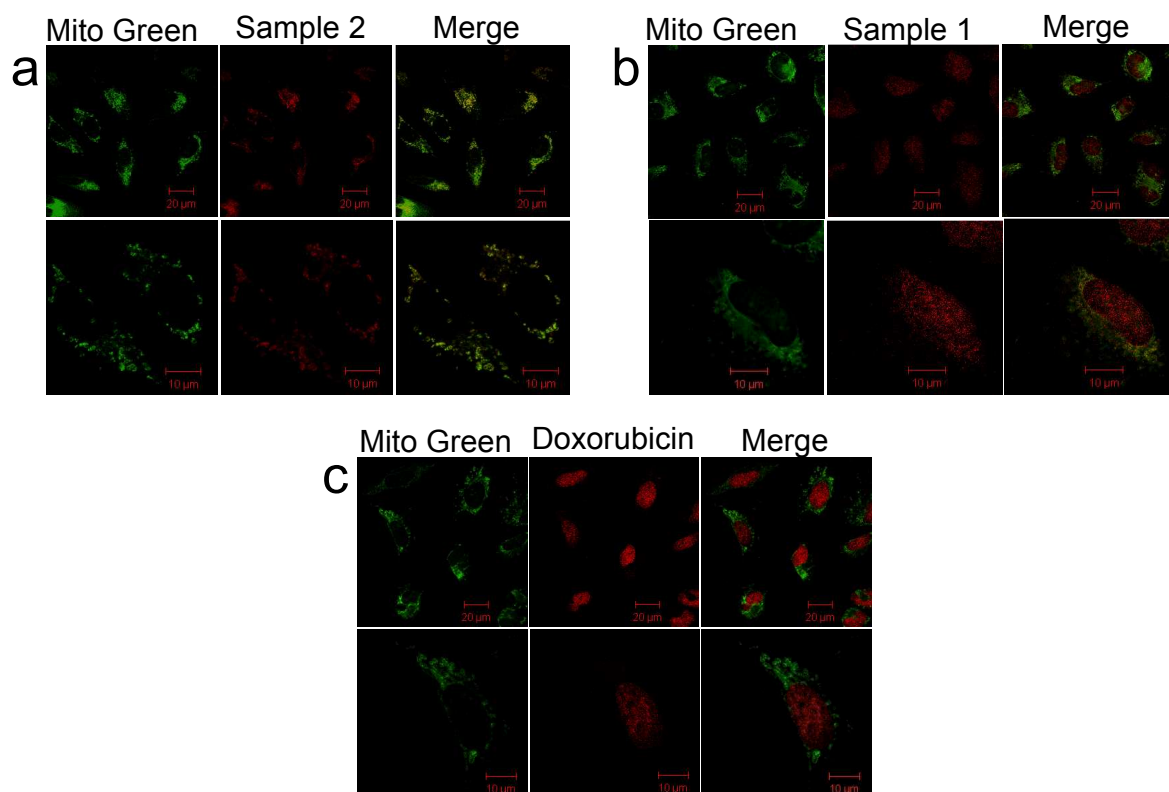


Figure 7. Cellular uptake of doxorubicin-loaded nanocapsules. (a) Cells treated with doxorubicin-loaded sample 2: green emission channel indicates the Mitotracker green staining of mitochondria within cells, red emission channel indicating the localization of doxorubicin-loaded nanocapsules. Here the doxorubicin remains encapsulated in the capsule core, indicates the capsule shell remains intact. (b) Cells treated with doxorubicin-loaded sample 1: green emission channel indicates the Mitotracker green staining of mitochondria within cells, red emission channel indicating the localization of doxorubicin-loaded nanocapsules and released doxorubicin. Right channel shows co-localization. The release of doxorubicin from the nanocapsule indicates the rupture of capsule shell membrane. (c) The control experiment with pure doxorubicin illustrating that doxorubicin passes through the cytosol and locates to the nucleus.

After ensuring the controlled release from the nanocapsule in the cellular model, experiments to analyze enzyme (EPL) triggered drug delivery within a widely employed vertebrate model (zebrafish embryo) were performed. Doxorubicin is expected to enhance the mortality of the zebrafish and thus, the in-vivo studies were performed using the fluorescent dye molecule

rhodamine 6G. Injection of 10 nl (500  $\mu\text{g}/\text{mL}$ ) of nanocapsule suspension at the one-cell stage of the embryos allows nanocapsules to disperse throughout the zebrafish cytoplasm (Figure S5). After 3 days (72 hours) incubation for Sample-2 (having polymeric backbone without ester linkage) with zebrafish, it was observed that the nanocapsules with entrapped rhodamine 6G were distributed throughout the fish body (Figure 8b), which resulted in a relatively weak emission intensity. Analogous experiments with Sample-1 showed a significantly enhanced emission intensity from rhodamine 6G (Figure 8c) throughout the zebrafish body. Literature reports reveal that the concentration of esterase enzyme is appreciable in the cytoplasm;<sup>71</sup> this induces release of the encapsulated rhodamine 6G within the zebrafish and prevents the self-quenching phenomenon operational for entrapped dye molecules. This confirms stimuli-responsive release of an encapsulated payload from the nanocapsule in a living vertebrate in real time.



Figure 8. *In-vivo* release experiment in zebrafish model. Bright-field (upper) and fluorescence (lower) images of zebrafish embryo after 72 hours of injection (a) control; (b) sample 2 and (c) sample 1. The injection was done at zero cell stage i.e, 0.5 hpf. Figure (b) shows rhodamine 6G remains encapsulated in the capsule core, indicates the capsule shell remains intact. Figure (c) shows that the release of rhodamine 6G from the capsule core by the degradation of esterase linkages of the capsule shell. In the control experiment, the equivalent amount of empty (without any payload) nanocapsules was injected. The scale bar is 0.6 mm.

The main goal in designing the NIPU nanocapsules was to make a material that could work as a fully degradable scaffold for drug release in a controlled manner. This function was evaluated in cell line experiment. Cell proliferation studies showed that cells treated with Sample -1 (300 nM drug) effectively limited the growth of cells by 56% relative to untreated cells (Figure 9b). Whereas the nanocapsules with non-ester linkages (Sample -2) loaded with 300 nM drug showed minimal effect on cell growth (Figure 9a). In control experiments, pure doxorubicin was used at a concentration of 300 nM. Taken together these experiments revealed that doxorubicin hydrochloride loaded NIPU nanocapsules display an enhanced therapeutic effect compared to free doxorubicin. This enhanced cancer cell killing efficacy may be due to mitochondria dysfunction caused by the delivered doxorubicin.<sup>72</sup>

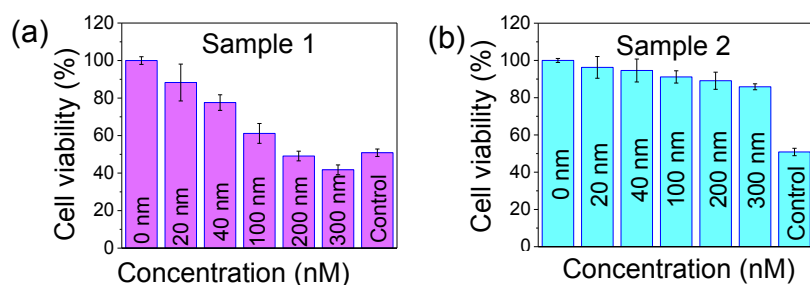


Figure 9. Evaluation of cell toxicity in LN229 cells in the presence of doxorubicin-loaded NIPU nanocapsules. Results indicate a limited effect after 24 h incubation from NIPU nanocapsules with an esterified linker (sample 1) in (a), and a dose-dependent decrease in cell viability with non-ester-linked NIPU nanocapsules (sample 2) in (b). Concentrations specify the effective concentration of doxorubicin that was loaded within the nanocapsules. Control is 300 nM free drug.

In addition, biocompatibility studies (MTT assay) with these nanocapsules were also evaluated and the results of such studies confirmed that these nanocapsules are nontoxic up to 100 micromolar concentrations (Figure S6 and S7). This clearly indicates that they are fully biocompatible, making them excellent candidates for biological applications.

## CONCLUSIONS

In summary, for the first time, we have shown a straightforward synthetic strategy toward a monodisperse drug carrier that offers itself to surface functionalization with mitochondria targeting ligands and can be degraded using esterase enzyme as an external trigger stimulus. The drug carriers is synthesized using the inverse mini-emulsion technique by exploiting an *in situ* NH<sub>2</sub>-carbonate green reaction at the droplet interface. The resulting nanocapsules can be loaded with hydrophilic small molecules, including dyes and drugs, for efficient enzyme-triggered release into cells and in vertebrate model (zebrafish). In addition, these nanocarriers can also be post grafted with organelle-specific targeting ligands for on-demand, target specific, drug delivery and bio-imaging. Such a formulation has the potential to be tailored to respond to a variety of stimuli through the systematic synthesis of different chemically unique monomers (e.g. azo linkages for photo-responsiveness). Through tailoring the post-grafting ligand the NIPU nanocapsule can be designed to target different organelle and release its encapsulated payload in a more biochemical specific fashion. These nanocarriers offer a promising novel therapeutic platform with high potential for biological imaging and drug delivery to fight cancer and other diseases..

## EXPERIMENTAL PROCEDURES

### Materials

All common chemicals and solvents that were used for the present study were procured from commercial suppliers and were used as received. Cyclohexane (> 99.0 %), dichloromethane (DCM) (> 99.0 %), triethylamine (TEA) (99.5 %), 1,4-Diaminobutane (99%), 1,8-Diaminooctane (98%), (5-Carboxypentyl)triphenylphosphonium bromide, esterase from porcine liver (EPL), DMEM cell culture media with L-glucose and Sodium bi carbonate, phosphate buffer saline (PBS), Fetal Bovine Serum, penicillin streptomycin, 4% paraformaldehyde

(PFA), vectashield h-1000 (Mounting agent), 50 mM ammonium chloride, mito tracker green, mito tracker deep red and Hoechst (33342) were purchased from Sigma Aldrich and were used without any further purification. Sodium chloride (KCl), penicillin/streptomycin (P/S) rhodamine green, rhodamine 6G and sodium dodecyl sulfate (SDS) were obtained from Fischer scientific and were used as received. Adipate bis carbonate and alkyl C10 diglycerol carbonate monomer were purchased from specific polymer (France). The block copolymer of hydrophobic polyhydroxy stearic acid and polyethylene glycol (molecular weight 20000 and was used as an emulsifier) were kindly supplied by Croda Europe Ltd. Minimum essential medium (MEM, containing HEPES and GlutaMAX supplement) was obtained from Thermo Fisher Scientific. Iscove's Modified Dulbecco's Medium (IMDM), Dulbecco's Modified Eagle's medium (DMEM), fetal calf serum (FCS), mouse monoclonal anti- $\alpha$ -tubulin antibody, Alexa Fluor® 488 Donkey Anti-Mouse IgG (H+L) antibody and 4',6-Diamidino-2-Phenylindole (DAPI) were bought at Life Technologies.

The 15 $\mu$ -slide 8 wells were bought at Ibidi. The culture plates and dark plates were obtained at Greiner Bio One. LN229 cells (glioblastoma, brain cancer) was purchased from ATCC. Water obtained from Sartorius Stedim biotech machine was used for the biological experiments.

### **Synthesis of Nanocapsules**

Nanocapsules containing hydrophilic payloads were typically prepared through an *in situ* reaction with selected monomers at a droplet interface using the inverse mini-emulsion process. For the synthesis of the polyurethane capsules, 83 mg (0.57 mmol) of 1,8-diaminooctane, 1.0 g of water, 1.0 mg of dye (rhodamine green or rhodamine 6G) or doxorubicin and 6.0 mg sodium chloride were added to 7 g of cyclohexane containing 200 mg of Hypermer™ B246. For pre-emulsification, the reaction mixture

was stirred at room temperature for 1 h at 1200 rpm. After that, the mini-emulsion was obtained by ultrasonication of the mixture using a Branson 450 W digital sonifier (1/4" tip) for 3 min (30 s pulse; 30 s pause).

An equimolar amount of bis carbonate moiety with respect to the amino monomer was dissolved in 4 g of the cyclohexane-dichloromethane mixture. To this, a catalytic amount of TEA was added. The reaction mixture was added in a dropwise manner to the above mentioned mini-emulsion dispersion, and the resulting mixture was left for stirring at room temperature 24h. The reaction mixture was then passed through a paper filter to separate any bulk product formed from the particulate dispersion. The milky dispersions (containing nanocapsules) were then directly used for the reaction.

### **Post-Grafting of Nanocapsules**

The post grafting of NIPU nanocapsules was performed using a modified procedure published previously.<sup>73</sup> Briefly, 2.0 g of NIPU nanocapsule dispersion (solid content of 5.0 wt %), (5-carboxypentyl)triphenylphosphonium cation (0.1 g), and 4-dimethylaminopyridine (0.05 g) were dissolved in 10 mL of dry DCM. N-ethyl-N'-(3-dimethylaminopropyl)carbodiimide hydrochloride (EDC.HCl) (0.08 g) was dissolved in CH<sub>2</sub>Cl<sub>2</sub> (1 mL) and added dropwise to the reaction mixture at 0 °C with stirring. The reaction mixture was allowed to for a8 h at room temperature, and then the nanocapsule solution was transferred into SDS water solution. The resulting dispersion was stirred at 1000 rpm for 2 h at room temperature. Subsequently, the reaction mixture was ultrasonicated for 10 min. This dispersion was left to stir overnight at 1000 rpm at room temperature. Then the redispersed solution was passed through the filter and dialyzed for an overnight before further use.

### **Dynamic Light Scattering (DLS)**

The average size and size distribution of the nanocapsules were measured at 20°C by DLS using Malvern Mastersizer 3000.

### **Fourier Transform Infrared Spectroscopy (FT-IR)**

The FT-IR spectroscopic measurements were carried out using an Agilent Cary 600 Series FTIR Spectrometers. The spectra were recorded in the range 400–4000  $\text{cm}^{-1}$  in KBr media.

### **High-Resolution Solid-State Nuclear Magnetic Resonance Spectroscopy**

The solid-state Carbon-13 CP/MAS NMR measurements were performed using a typical procedure described elsewhere.<sup>59</sup> For the material composition analysis, solid-state Carbon-13 CP/MAS NMR spectra were acquired on a Bruker, Avance II (125 MHz) spectrometer (9.4 T wide bore magnet) equipped with a 1.3 mm MAS probe. The aromatic signal of hexamethyl benzene was used to determine the Hartmann-Hahn condition ( $\omega_{1H} = \gamma_H B_{1H} = \gamma_C B_{1C} = \omega_{1C}$ ) for cross-polarization (CP), and to calibrate the carbon chemical shift scale (132.1 ppm).

### **Electron Microscopy**

Transmission electronic microscope (TEM) images were collected using a JEOL JEM 2100 microscope operated at 200 kV. The morphology of the nanocapsules was studied by placing a dilute dispersion of the respective nanocapsule sample on the TEM grids (lacey carbon formvar-coated Cu (300 mesh)) using transmission electron

microscopy. No additional staining was used. Scanning electron micrographs (SEM) were obtained using ZEISS SUORA 35 VP scanning electron microscope.

### ***In-vitro* Esterase Cleavage Assay**

The doxorubicin loaded nanocapsules, prepared by the inverse-mini-emulsion technique, were redispersed in HEPES buffer at pH 7.4 and esterase (Porcine liver esterase, Sigma Aldrich, 5 units) was added and the release of doxorubicin as a function of time was studied using fluorescence spectroscopy (for doxorubicin  $\lambda_{\text{Max}}^{\text{Abs}} = 486 \text{ nm}$ ,  $\lambda_{\text{Max}}^{\text{Ems}} = 590 \text{ nm}$ ). It is important to note that the fluorescence of the doxorubicin moiety was partially quenched when it is entrapped inside the nanocapsules and this is attributed to a self-quenching phenomenon. The analogous concentration of the respective fluorophore showed strong fluorescence when existed in solution phase, as this nullified the self-quenching process. This relative change in fluorescence allowed us to evaluate the relative distribution of doxorubicin in solution and the entrapped state, respectively. The percentage of released doxorubicin was calculated with respect to the amount of encapsulated doxorubicin by the nanocapsule. The encapsulation efficiency of nanocapsules was evaluated following a previously reported protocol.<sup>74</sup> A reference sample of nanocapsule dispersion (without any doxorubicin entrapped inside the nanocapsules) was used for control studies and it was prepared using the exact protocol that was followed for the doxorubicin-loaded nanocapsule dispersion. The resulting nanocapsule dispersion was redispersed in an aqueous SDS (0.5 wt.%) solution containing an equal amount of doxorubicin used in the encapsulation experiment. The resultant solution was centrifuged and diluted properly prior to fluorescence measurement. The fluorescence intensity signal of the reference sample was set as 100%. The amount of non-encapsulated doxorubicin was estimated by measuring the difference in fluorescent intensities between the

supernatants collected after centrifugation (12000 rpm, 20 min, 4°C), from the reference and doxorubicin encapsulated nanocapsule sample. The measurement was done in triplicate, and an average value of three data was used for evaluation. The percentage of doxorubicin release caused by Porcine liver esterase was evaluated by using the following equation:

$$\% \text{ of release} = \frac{F_t}{F_o} \times 100$$

Where  $F_t$  is the time-dependent fluorescence intensity of supernatant sample and  $F_o$  is the fluorescence intensity of the reference.

### **Optical Microscopy**

LN229 cells were seeded on coverslips (22 mm x 22 mm,  $170 \pm 5 \mu\text{m}$  square cover glasses) placed in six-well plates in DMEM culture medium containing (10% FBS and 1% Penicillin-Streptomycin) for 24 hours at 37 °C, 5 % CO<sub>2</sub>. After 24 hours when 70% confluency was achieved, these cells were washed thrice with DMEM culture medium. After that cells were washed again twice with PBS. After live cell uptake for 12 hours, the cells were washed with DMEM media and fixed with 4% PFA for 15 minutes and then washed with PBS, the coverslips were mounted using the mounting medium (Vectashield h-1000). The coverslips were sealed using nail varnish and the sample was then imaged. All microscopic studies were carried out using a Delta Vision OMX-SIM microscope running in deconvoluted wide-field or SIM mode. Image processing was carried out by using the Soft Worx software.

### **Cellular Uptake and Confocal Imaging of Doxorubicin-Loaded Nanocapsules**

LN229 cells were grown in 10% FBS in DMEM with 1% Penicillin/Streptomycin. Confluent cells were treated with 50  $\mu\text{g}/\text{mL}$  of doxorubicin-loaded nanocapsules for 24 hours at 37 °C. Cells were treated with 500 nM Mitotracker Green for 20 minutes

before 24 hours were over. Then the cells were washed for six times with 1X PBS buffer for removing the surface adsorbed compounds. Cells were fixed using chilled methanol for 15 minutes at -20°C and then rehydrated for 30 minutes with PBS 1X buffer at room temperature. After washing the cells with PBS 1X thrice, the coverslips were mounted on glass-slides using the mounting medium. Fluorescence was observed in Zeiss confocal microscope.

### **Doxorubicin Treatment**

LN229 cells (confluent) were incubated with 75 µg/mL, 50 µg/mL, 25 µg/mL, 10 µg/mL and 5 µg/mL of nanocapsules containing 0.22 wt % of doxorubicin drug. Equivalent concentrations of free doxorubicin were incubated as a positive control. The same concentrations of nanocapsules without doxorubicin were incubated as a negative control. Incubation time was 24 hours in all the above cases.

### **Zebrafish Maintenance and Embryo Harvesting**

Zebrafish were maintained according to the approved guidelines of Centre for Cellular and Molecular Biology, Hyderabad Animal Ethics Committee and good laboratory practice developed in-house. Zebrafish (strain *Danio rerio*) were purchased from the local market and maintained them at a constant temperature of 25 °C and pH 7.4 with a 12/12 h dark/light cycle. For spawning, one adult male and two female fish were chosen and placed at opposite sides of a small breeding tank separated by a tank divider, at 18.00 of the previous day of the experiment. On the next day, the tank divider was removed at 10:30 and allowed the fish to breed for 10 min and checked for embryos. Embryos were collected immediately and these were transferred to the embryo media E3 (50mM NaCl, 0.17mM KCl, 0.33mM CaCl<sub>2</sub>, 0.33mM MgSO<sub>4</sub>) and were used for further experimentations.

### **Zebrafish Injections and Fluorescence imaging**

Zebrafish embryos were injected using a glass needle controlled with a micromanipulator which is connected to an Eppendorf FemtoJet express. Microscopic visualization of the zebrafish during the injections was aided by Zeiss Axiovert 100 inverted microscope. To study nanocapsule behavior (control release of encapsulated payload) in zebrafish embryos, 10 nl (500 µg/ mL) of nanocapsule suspension was injected in 0.5 hpf (hours post fertilization) embryos. The zebrafish embryos (0.5 hpf) were used at the one-cell stage to ensure that the nanocapsules are permeated into the embryos and dispersed throughout the zebrafish cytoplasm. Following this, the zebrafish embryos were transferred to embryo media E3 and kept in an incubator for 72 hours. Prior to imaging zebrafish embryos were anesthetized by adding tricaine to embryo water. Upon imaging, embryos were placed on a glass slide with just enough embryo water to avoid drying the embryo. This glass slide was viewed through a fluorescent stereomicroscope (Leica M165 FC, Leica Microsystems, Heerbrug, Switzerland).

### **MTT Assay**

The redispersed nanocapsule solution was tested for cytotoxicity by MTT assay. The nanocapsules were washed with HEPES buffer in order to remove the excess of surfactant by multiple centrifugation and redispersion (20 times). LN229 cells (Glioblastoma cell line) ( $5 \times 10^3$ ) were seeded in a 96 well plate in DMEM medium (Gibco) supplemented with 5% Fetal Bovine Serum along with 100 Units of penicillin-streptomycin antibiotics. Cells were treated with 100 µg/mL, 75 µg/mL, 50 µg/mL, 25 µg/mL and 10 µg/mL of nanocapsules and incubated at 37 °C in a 5 % CO<sub>2</sub> incubator. After incubation for 24 h, nanocapsules treated cells were washed thrice with 1xPBS. The concentration range employed for the present study was based on literature value that was typically used for cell studies using nanocapsules.<sup>75</sup> MTT reagent (0.5 mg/ml) was added to the cells and incubated for 4 hours

more at 37°C. The media was then removed and formazan crystals formed were dissolved in DMSO. Percentage of cell death was determined by measuring the absorbance reading of the formazan at 570 nm. The experiment was done in triplicates.

## **ASSOCIATED CONTENT**

Supporting Information:

Experiment details of concentration dependent cell-dependent uptake of nanocapsules. Co-localization studies and MTT assay.

## **AUTHOR INFORMATION**

Corresponding Author

Email: [sumitpramanik@csmcri.res.in](mailto:sumitpramanik@csmcri.res.in)

[a.das@csmcri.res.in](mailto:a.das@csmcri.res.in)

[James.thomas@sheffield.ac.uk](mailto:James.thomas@sheffield.ac.uk)

Notes

The authors declare no competing financial interest.

## **ACKNOWLEDGMENTS**

AD acknowledges SERB grants (EMR/2016/001850 & JCB/2017/000004) and DBT (India) grant BT/PR22251/NNT/ 28/1274/2017) for financial support. SKP acknowledges SERB (PDF/2015/000745) for financial support. Some of the imaging work was performed at the

Wolfson Light Microscopy Facility, using the super resolution OMX SIM microscope. JAT and SS acknowledge an MRC grant (MK/K0157531/1) for this facility. SS is also grateful to the University of Sheffield, Imaging Life initiative for a studentship.

## REFERENCES

- (1) Xiao, H.; Li, P.; Zhang, W.; Tang, B. An ultrasensitive near-infrared ratiometric fluorescent probe for imaging mitochondrial polarity in live cells and in vivo. *Chemical Science* **2016**, *7* (2), 1588-1593, DOI: 10.1039/C5SC04099J.
- (2) Hoye, A. T.; Davoren, J. E.; Wipf, P.; Fink, M. P.; Kagan, V. E. Targeting Mitochondria. *Accounts of Chemical Research* **2008**, *41* (1), 87-97, DOI: 10.1021/ar700135m.
- (3) Huang, H.; Zhang, P.; Qiu, K.; Huang, J.; Chen, Y.; Ji, L.; Chao, H. Mitochondrial Dynamics Tracking with Two-Photon Phosphorescent Terpyridyl Iridium(III) Complexes. *Scientific Reports* **2016**, *6*, 20887, DOI: 10.1038/srep20887  
<https://www.nature.com/articles/srep20887#supplementary-information>.
- (4) Hajnóczky, G.; Csordás, G.; Das, S.; Garcia-Perez, C.; Saotome, M.; Sinha Roy, S.; Yi, M. Mitochondrial calcium signalling and cell death: Approaches for assessing the role of mitochondrial Ca<sup>2+</sup> uptake in apoptosis. *Cell Calcium* **2006**, *40* (5-6), 553-560, DOI: <https://doi.org/10.1016/j.ceca.2006.08.016>.
- (5) Fulda, S.; Galluzzi, L.; Kroemer, G. Targeting mitochondria for cancer therapy. *Nat Rev Drug Discov* **2010**, *9* (6), 447-464, DOI: [http://www.nature.com/nrd/journal/v9/n6/supinfo/nrd3137\\_S1.html](http://www.nature.com/nrd/journal/v9/n6/supinfo/nrd3137_S1.html).
- (6) Biswas, S.; Torchilin, V. P. Nanopreparations for organelle-specific delivery in cancer. *Advanced Drug Delivery Reviews* **2014**, *66*, 26-41, DOI: <https://doi.org/10.1016/j.addr.2013.11.004>.
- (7) Ju, E.; Li, Z.; Liu, Z.; Ren, J.; Qu, X. Near-Infrared Light-Triggered Drug-Delivery Vehicle for Mitochondria-Targeted Chemo-Photothermal Therapy. *ACS Applied Materials & Interfaces* **2014**, *6* (6), 4364-4370, DOI: 10.1021/am5000883.
- (8) Solomon, M. A.; Shah, A. A.; D'Souza, G. G. M. In Vitro assessment of the utility of stearyl triphenyl phosphonium modified liposomes in overcoming the resistance of ovarian carcinoma Ovar-3 cells to paclitaxel. *Mitochondrion* **2013**, *13* (5), 464-472, DOI: <https://doi.org/10.1016/j.mito.2012.10.013>.
- (9) Lesnefsky, E. J.; Moghaddas, S.; Tandler, B.; Kerner, J.; Hoppel, C. L. Mitochondrial Dysfunction in Cardiac Disease: Ischemia-Reperfusion, Aging, and Heart Failure. *Journal of Molecular and Cellular Cardiology* **2001**, *33* (6), 1065-1089, DOI: <https://doi.org/10.1006/jmcc.2001.1378>.
- (10) Tompkins, A. J.; Burwell, L. S.; Digerness, S. B.; Zaragoza, C.; Holman, W. L.; Brookes, P. S. Mitochondrial dysfunction in cardiac ischemia-reperfusion injury: ROS from complex I, without inhibition. *Biochimica et Biophysica Acta (BBA) - Molecular Basis of Disease* **2006**, *1762* (2), 223-231, DOI: <https://doi.org/10.1016/j.bbadis.2005.10.001>.
- (11) Ann, G.; Richard, G. B. Is a "Mitochondrial Psychiatry" in the Future? A Review. *Current Psychiatry Reviews* **2005**, *1* (3), 255-271, DOI: <http://dx.doi.org/10.2174/157340005774575064>.
- (12) Lin, M. T.; Beal, M. F. Mitochondrial dysfunction and oxidative stress in neurodegenerative diseases. *Nature* **2006**, *443* (7113), 787-795.
- (13) Kulkarni, P. S.; Haldar, M. K.; Confeld, M. I.; Langaas, C. J.; Yang, X.; Qian, S. Y.; Mallik, S. Mitochondria-targeted fluorescent polymersomes for drug delivery to cancer cells. *Polymer chemistry* **2016**, *7* (25), 4151-4154, DOI: 10.1039/C6PY00623J.
- (14) Rin Jean, S.; Tulumello, D. V.; Wisnovsky, S. P.; Lei, E. K.; Pereira, M. P.; Kelley, S. O. Molecular Vehicles for Mitochondrial Chemical Biology and Drug Delivery. *ACS Chemical Biology* **2014**, *9* (2), 323-333, DOI: 10.1021/cb400821p.
- (15) Wang, L.; Liu, Y.; Li, W.; Jiang, X.; Ji, Y.; Wu, X.; Xu, L.; Qiu, Y.; Zhao, K.; Wei, T.; Li, Y.; Zhao, Y.; Chen, C. Selective Targeting of Gold Nanorods at the Mitochondria of Cancer Cells: Implications for Cancer Therapy. *Nano Letters* **2011**, *11* (2), 772-780, DOI: 10.1021/nl103992v.
- (16) Boddapati, S. V.; D'Souza, G. G. M.; Erdogan, S.; Torchilin, V. P.; Weissig, V. Organelle-Targeted Nanocarriers: Specific Delivery of Liposomal Ceramide to Mitochondria Enhances Its Cytotoxicity in Vitro and in Vivo. *Nano Letters* **2008**, *8* (8), 2559-2563, DOI: 10.1021/nl801908y.
- (17) Biswas, S.; Dodwadkar, N. S.; Piroyan, A.; Torchilin, V. P. Surface conjugation of triphenylphosphonium to target poly(amidoamine) dendrimers to mitochondria. *Biomaterials* **2012**, *33* (18), 4773-4782, DOI: 10.1016/j.biomaterials.2012.03.032.
- (18) Marrache, S.; Dhar, S. Engineering of blended nanoparticle platform for delivery of mitochondria-acting therapeutics. *Proceedings of the National Academy of Sciences of the United States of America* **2012**, *109* (40), 16288-16293, DOI: 10.1073/pnas.1210096109.

- (19) Wang, X.-H.; Peng, H.-S.; Yang, L.; You, F.-T.; Teng, F.; Tang, A.-W.; Zhang, F.-J.; Li, X.-H. Poly-L-lysine assisted synthesis of core-shell nanoparticles and conjugation with triphenylphosphonium to target mitochondria. *Journal of Materials Chemistry B* **2013**, *1* (38), 5143-5152, DOI: 10.1039/C3TB20884B.
- (20) Marrache, S.; Tundup, S.; Harn, D. A.; Dhar, S. Ex Vivo Programming of Dendritic Cells by Mitochondria-Targeted Nanoparticles to Produce Interferon-Gamma for Cancer Immunotherapy. *ACS Nano* **2013**, *7* (8), 7392-7402, DOI: 10.1021/nn403158n.
- (21) Liu, B.; Shah, M.; Zhang, G.; Liu, Q.; Pang, Y. Biocompatible Flavone-Based Fluorogenic Probes for Quick Wash-Free Mitochondrial Imaging in Living Cells. *ACS Applied Materials & Interfaces* **2014**, *6* (23), 21638-21644, DOI: 10.1021/am506698f.
- (22) Mura, S.; Nicolas, J.; Couvreur, P. Stimuli-responsive nanocarriers for drug delivery. *Nat Mater* **2013**, *12* (11), 991-1003, DOI: 10.1038/nmat3776.
- (23) Yan, M.; Liang, M.; Wen, J.; Liu, Y.; Lu, Y.; Chen, I. S. Y. Single siRNA Nanocapsules for Enhanced RNAi Delivery. *Journal of the American Chemical Society* **2012**, *134* (33), 13542-13545, DOI: 10.1021/ja304649a.
- (24) Chen, C.-K.; Law, W.-C.; Aalinkeel, R.; Yu, Y.; Nair, B.; Wu, J.; Mahajan, S.; Reynolds, J. L.; Li, Y.; Lai, C. K.; Tzanakakis, E. S.; Schwartz, S. A.; Prasad, P. N.; Cheng, C. Biodegradable cationic polymeric nanocapsules for overcoming multidrug resistance and enabling drug-gene co-delivery to cancer cells. *Nanoscale* **2014**, *6* (3), 1567-1572, DOI: 10.1039/C3NR04804G.
- (25) Wang, X.; Hu, J.; Liu, G.; Tian, J.; Wang, H.; Gong, M.; Liu, S. Reversibly Switching Bilayer Permeability and Release Modules of Photochromic Polymersomes Stabilized by Cooperative Noncovalent Interactions. *Journal of the American Chemical Society* **2015**, *137* (48), 15262-15275, DOI: 10.1021/jacs.5b10127.
- (26) He, H.; Chen, Y.; Li, Y.; Song, Z.; Zhong, Y.; Zhu, R.; Cheng, J.; Yin, L. Effective and Selective Anti-Cancer Protein Delivery via All-Functions-in-One Nanocarriers Coupled with Visible Light-Responsive, Reversible Protein Engineering. *Advanced Functional Materials*, 1706710-n/a, DOI: 10.1002/adfm.201706710.
- (27) Liao, W.-C.; Willner, I. Synthesis and Applications of Stimuli-Responsive DNA-Based Nano- and Micro-Sized Capsules. *Advanced Functional Materials* **2017**, *27* (41), 1702732-n/a, DOI: 10.1002/adfm.201702732.
- (28) Kang, B.; Opatz, T.; Landfester, K.; Wurm, F. R. Carbohydrate nanocarriers in biomedical applications: functionalization and construction. *Chemical Society Reviews* **2015**, *44* (22), 8301-8325, DOI: 10.1039/C5CS00092K.
- (29) Sharma, S.; Paiphansiri, U.; Hombach, V.; Mailänder, V.; Zimmermann, O.; Landfester, K.; Rasche, V. Characterization of MRI contrast agent-loaded polymeric nanocapsules as versatile vehicle for targeted imaging. *Contrast Media & Molecular Imaging* **2010**, *5* (2), 59-69, DOI: 10.1002/cmml.364.
- (30) Jiang, S.; Landfester, K.; Crespy, D. Control of the release of functional payloads from redox-responsive nanocapsules. *RSC Advances* **2016**, *6* (106), 104330-104337, DOI: 10.1039/C6RA22733C.
- (31) Behzadi, S.; Steinmann, M.; Estupiñán, D.; Landfester, K.; Crespy, D. The pro-active payload strategy significantly increases selective release from mesoporous nanocapsules. *Journal of Controlled Release* **2016**, *242*, 119-125, DOI: <http://doi.org/10.1016/j.jconrel.2016.08.040>.
- (32) Tian, H.; Du, J.; Wen, J.; Liu, Y.; Montgomery, S. R.; Scott, T. P.; Aghdasi, B.; Xiong, C.; Suzuki, A.; Hayashi, T.; Ruangchainikom, M.; Phan, K.; Weintraub, G.; Raed, A.; Murray, S. S.; Daubs, M. D.; Yang, X.; Yuan, X.-b.; Wang, J. C.; Lu, Y. Growth-Factor Nanocapsules That Enable Tunable Controlled Release for Bone Regeneration. *ACS Nano* **2016**, *10* (8), 7362-7369, DOI: 10.1021/acs.nano.5b07950.
- (33) Chen, N.; Dempere, L. A.; Tong, Z. Synthesis of pH-Responsive Lignin-Based Nanocapsules for Controlled Release of Hydrophobic Molecules. *ACS Sustainable Chemistry & Engineering* **2016**, *4* (10), 5204-5211, DOI: 10.1021/acssuschemeng.6b01209.
- (34) Hofmeister, I.; Landfester, K.; Taden, A. pH-Sensitive Nanocapsules with Barrier Properties: Fragrance Encapsulation and Controlled Release. *Macromolecules* **2014**, *47* (16), 5768-5773, DOI: 10.1021/ma501388w.
- (35) Brannigan, R. P.; Dove, A. P. Synthesis, properties and biomedical applications of hydrolytically degradable materials based on aliphatic polyesters and polycarbonates. *Biomaterials Science* **2017**, *5* (1), 9-21, DOI: 10.1039/C6BM00584E.
- (36) Tong, R.; Gabrielson, N. P.; Fan, T. M.; Cheng, J. Polymeric Nanomedicines Based on Poly(lactide) and Poly(lactide-co-glycolide). *Current opinion in solid state & materials science* **2012**, *16* (6), 323-332, DOI: 10.1016/j.cossms.2013.01.001.
- (37) Chan, B. Q. Y.; Heng, S. J. W.; Liow, S. S.; Zhang, K.; Loh, X. J. Dual-responsive hybrid thermoplastic shape memory polyurethane. *Materials Chemistry Frontiers* **2017**, *1* (4), 767-779, DOI: 10.1039/C6QM00243A.
- (38) Zhang, Z.-x.; Dou, J.-x.; He, J.-h.; Xiao, C.-x.; Shen, L.-y.; Yang, J.-h.; Wang, Y.; Zhou, Z.-w. Electrically/infrared actuated shape memory composites based on a bio-based polyester blend and graphene nanoplatelets and their excellent self-driven ability. *Journal of Materials Chemistry C* **2017**, DOI: 10.1039/C7TC00828G.
- (39) Ihata, O.; Kayaki, Y.; Ikariya, T. Synthesis of Thermoresponsive Polyurethane from 2-Methylaziridine and Supercritical Carbon Dioxide. *Angewandte Chemie International Edition* **2004**, *43* (6), 717-719, DOI: 10.1002/anie.200352215.
- (40) Remon, J. P.; Vervaet, C., Polyurethanes as oral drug delivery platform. Google Patents: 2016.
- (41) Hunter, W.; Gravett, D.; Toleikis, P.; Maiti, A.; Signore, P.; Liggins, R., Medical implants and anti-scarring agents. Google Patents: 2005.
- (42) Yongabi, D.; Khorshid, M.; Losada-Pérez, P.; Eersels, K.; Deschaume, O.; D'Haen, J.; Bartic, C.; Hooyberghs, J.; Thoelen, R.; Wübbenhorst, M.; Wagner, P. Cell detection by surface imprinted polymers SIPs: A study to unravel the recognition mechanisms. *Sensors and Actuators B: Chemical* **2018**, *255*, 907-917, DOI: <https://doi.org/10.1016/j.snb.2017.08.122>.
- (43) Kathalewar, M. S.; Joshi, P. B.; Sabnis, A. S.; Malshe, V. C. Non-isocyanate polyurethanes: from chemistry to applications. *RSC Advances* **2013**, *3* (13), 4110-4129, DOI: 10.1039/C2RA21938G.

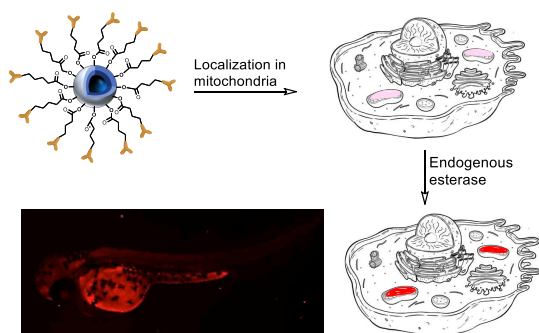
- (44) Rokicki, G.; Parzuchowski, P. G.; Mazurek, M. Non-isocyanate polyurethanes: synthesis, properties, and applications. *Polymers for Advanced Technologies* **2015**, *26* (7), 707-761, DOI: 10.1002/pat.3522.
- (45) Maisonneuve, L.; Lamarzelle, O.; Rix, E.; Grau, E.; Cramail, H. Isocyanate-Free Routes to Polyurethanes and Poly(hydroxy Urethane)s. *Chemical Reviews* **2015**, *115* (22), 12407-12439, DOI: 10.1021/acs.chemrev.5b00355.
- (46) Kreye, O.; Mutlu, H.; Meier, M. A. R. Sustainable routes to polyurethane precursors. *Green Chemistry* **2013**, *15* (6), 1431-1455, DOI: 10.1039/C3GC40440D.
- (47) Delebecq, E.; Pascault, J.-P.; Boutevin, B.; Ganachaud, F. On the Versatility of Urethane/Urea Bonds: Reversibility, Blocked Isocyanate, and Non-isocyanate Polyurethane. *Chemical Reviews* **2013**, *113* (1), 80-118, DOI: 10.1021/cr300195n.
- (48) Toumia, Y.; Domenici, F.; Orlanducci, S.; Mura, F.; Grishenkov, D.; Trochet, P.; Lacerenza, S.; Bordi, F.; Paradossi, G. Graphene Meets Microbubbles: A Superior Contrast Agent for Photoacoustic Imaging. *ACS Applied Materials & Interfaces* **2016**, *8* (25), 16465-16475, DOI: 10.1021/acsami.6b04184.
- (49) Ruan, H.; Jang, M.; Yang, C. Optical focusing inside scattering media with time-reversed ultrasound microbubble encoded light. *Nature Communications* **2015**, *6*, 8968, DOI: 10.1038/ncomms9968
- <https://www.nature.com/articles/ncomms9968#supplementary-information>.
- (50) Peng, Y.; Xiong, B.; Peng, L.; Li, H.; He, Y.; Yeung, E. S. Recent Advances in Optical Imaging with Anisotropic Plasmonic Nanoparticles. *Analytical Chemistry* **2015**, *87* (1), 200-215, DOI: 10.1021/ac504061p.
- (51) Coll, J.-L. Cancer optical imaging using fluorescent nanoparticles. *Nanomedicine (London, England)* **2011**, *6* (1), 7-10, DOI: 10.2217/nnm.10.144.
- (52) Gao, X.; Cui, Y.; Levenson, R. M.; Chung, L. W. K.; Nie, S. In vivo cancer targeting and imaging with semiconductor quantum dots. *Nat Biotech* **2004**, *22* (8), 969-976, DOI: [http://www.nature.com/nbt/journal/v22/n8/supinfo/nbt994\\_S1.html](http://www.nature.com/nbt/journal/v22/n8/supinfo/nbt994_S1.html).
- (53) Shang, L.; Gao, P.; Wang, H.; Popescu, R.; Gerthsen, D.; Nienhaus, G. U. Protein-based fluorescent nanoparticles for super-resolution STED imaging of live cells. *Chemical Science* **2017**, *8* (3), 2396-2400, DOI: 10.1039/C6SC04664A.
- (54) Nienhaus, K.; Ulrich Nienhaus, G. Fluorescent proteins for live-cell imaging with super-resolution. *Chemical Society Reviews* **2014**, *43* (4), 1088-1106, DOI: 10.1039/C3CS60171D.
- (55) Hell, S. W. Far-Field Optical Nanoscopy. *Science* **2007**, *316* (5828), 1153.
- (56) Caruso, F.; Caruso, R. A.; Möhwald, H. Nanoengineering of Inorganic and Hybrid Hollow Spheres by Colloidal Templating. *Science* **1998**, *282* (5391), 1111-1114, DOI: 10.1126/science.282.5391.1111.
- (57) Antonietti, M.; Basten, R.; Lohmann, S. Polymerization in microemulsions — a new approach to ultrafine, highly functionalized polymer dispersions. *Macromolecular Chemistry and Physics* **1995**, *196* (2), 441-466, DOI: 10.1002/macp.1995.021960201.
- (58) Landfester, K. Miniemulsion Polymerization and the Structure of Polymer and Hybrid Nanoparticles. *Angewandte Chemie International Edition* **2009**, *48* (25), 4488-4507, DOI: 10.1002/anie.200900723.
- (59) Kuypers, S.; Pramanik, S. K.; D'Olieslaeger, L.; Reekmans, G.; Peters, M.; D'Haen, J.; Vanderzande, D.; Junkers, T.; Adriaensens, P.; Ethirajan, A. Interfacial thiol-isocyanate reactions for functional nanocarriers: a facile route towards tunable morphologies and hydrophilic payload encapsulation. *Chemical Communications* **2015**, *51* (87), 15858-15861, DOI: 10.1039/C5CC05258K.
- (60) Field, L. D.; Delehanty, J. B.; Chen, Y.; Medintz, I. L. Peptides for Specifically Targeting Nanoparticles to Cellular Organelles: Quo Vadis? *Accounts of Chemical Research* **2015**, *48* (5), 1380-1390, DOI: 10.1021/ar500449v.
- (61) Jean, S. R.; Ahmed, M.; Lei, E. K.; Wisnovsky, S. P.; Kelley, S. O. Peptide-Mediated Delivery of Chemical Probes and Therapeutics to Mitochondria. *Accounts of Chemical Research* **2016**, *49* (9), 1893-1902, DOI: 10.1021/acs.accounts.6b00277.
- (62) Zielonka, J.; Joseph, J.; Sikora, A.; Hardy, M.; Ouari, O.; Vasquez-Vivar, J.; Cheng, G.; Lopez, M.; Kalyanaraman, B. Mitochondria-Targeted Triphenylphosphonium-Based Compounds: Syntheses, Mechanisms of Action, and Therapeutic and Diagnostic Applications. *Chemical Reviews* **2017**, *117* (15), 10043-10120, DOI: 10.1021/acs.chemrev.7b00042.
- (63) Losada-Pérez, P.; Khorshid, M.; Renner, F. U. Interactions of Aqueous Imidazolium-Based Ionic Liquid Mixtures with Solid-Supported Phospholipid Vesicles. *PLOS ONE* **2016**, *11* (9), e0163518, DOI: 10.1371/journal.pone.0163518.
- (64) Panariti, A.; Miserocchi, G.; Rivolta, I. The effect of nanoparticle uptake on cellular behavior: disrupting or enabling functions? *Nanotechnology, Science and Applications* **2012**, *5*, 87-100, DOI: 10.2147/NSA.S25515.
- (65) Rosenbauer, E.-M.; Wagner, M.; Musyanovych, A.; Landfester, K. Controlled Release from Polyurethane Nanocapsules via pH-, UV-Light- or Temperature-Induced Stimuli. *Macromolecules* **2010**, *43* (11), 5083-5093, DOI: 10.1021/ma100481s.
- (66) Flores, J. D.; Shin, J.; Hoyle, C. E.; McCormick, C. L. Direct RAFT polymerization of an unprotected isocyanate-containing monomer and subsequent structionpendant functionalization using "click"-type reactions. *Polymer Chemistry* **2010**, *1* (2), 213-220, DOI: 10.1039/B9PY00294D.
- (67) Lee, J.-M.; Kim, S.-H.; Jeong, H.-Y.; Ahn, N.-R.; Roh, H.-G.; Cho, J.-W.; Chun, B.-C.; Oh, S.-T.; Park, J.-S. Preparation and characterization of polyurethane foam using a PLA/PEG polyol mixture. *Fibers and Polymers* **2014**, *15* (7), 1349-1356, DOI: 10.1007/s12221-014-1349-7.
- (68) Spěváček, J.; Brus, J.; Divers, T.; Grohens, Y. Solid-state NMR study of biodegradable starch/polycaprolactone blends. *European Polymer Journal* **2007**, *43* (5), 1866-1875, DOI: <http://doi.org/10.1016/j.eurpolymj.2007.02.021>.
- (69) Moreland, J. C.; Wilkes, G. L.; Moreland, C. G.; Sankar, S. S.; Stejskal, E. O.; Turner, R. B. Solid-state NMR characterization of motion in flexible polyurethane foams. *Journal of Applied Polymer Science* **1994**, *52* (9), 1175-1180, DOI: 10.1002/app.1994.070520901.

- (70) Teng, Z.; Wang, C.; Tang, Y.; Li, W.; Bao, L.; Zhang, X.; Su, X.; Zhang, F.; Zhang, J.; Wang, S.; Zhao, D.; Lu, G. Deformable Hollow Periodic Mesoporous Organosilica Nanocapsules for Significantly Improved Cellular Uptake. *Journal of the American Chemical Society* **2018**, *140* (4), 1385-1393, DOI: 10.1021/jacs.7b10694.
- (71) Tokudome, Y.; Katayanagi, M.; Hashimoto, F. Esterase Activity and Intracellular Localization in Reconstructed Human Epidermal Cultured Skin Models. *Annals of Dermatology* **2015**, *27* (3), 269-274, DOI: 10.5021/ad.2015.27.3.269.
- (72) Qu, Q.; Ma, X.; Zhao, Y. Targeted delivery of doxorubicin to mitochondria using mesoporous silica nanoparticle nanocarriers. *Nanoscale* **2015**, *7* (40), 16677-16686, DOI: 10.1039/C5NR05139H.
- (73) Tsakos, M.; Schaffert, E. S.; Clement, L. L.; Villadsen, N. L.; Poulsen, T. B. Ester coupling reactions - an enduring challenge in the chemical synthesis of bioactive natural products. *Natural Product Reports* **2015**, *32* (4), 605-632, DOI: 10.1039/C4NP00106K.
- (74) Siebert, J. M.; Baier, G.; Musyanovych, A.; Landfester, K. Towards copper-free nanocapsules obtained by orthogonal interfacial "click" polymerization in miniemulsion. *Chemical Communications* **2012**, *48* (44), 5470-5472, DOI: 10.1039/C2CC30253E.
- (75) Pramanik, S. K.; Sreedharan, S.; Singh, H.; Green, N. H.; Smythe, C.; Thomas, J. A.; Das, A. Imaging cellular trafficking processes in real time using lysosome targeted up-conversion nanoparticles. *Chemical Communications* **2017**, *53* (94), 12672-12675, DOI: 10.1039/C7CC08185E.

## Table of Contents:

### Mitochondria Targeting Non-isocyanate-based Polyurethane Nanocapsules for Enzyme-Triggered Drug Release

Sumit Kumar Pramanik, Sreejesh Sreedharan, Harwinder Singh, Mohsina Khan, Karishma Tiwari, Anjali Shiras, Carl Smythe, Jim. A. Thomas and Amitava Das



Biodegradable polyurethane nanocapsules for endogenous enzyme induced release of encapsulated doxorubicin or fluorescent dye in mitochondria for improved efficacy.